AGU PUBLICATIONS

JGR

Journal of Geophysical Research: Space Physics

RESEARCH ARTICLE
10.1002/2017JA024325

Key Points:
- Persistent enhancements to the southeast in *F* layer ionization and airglow due to an unusual poleward excursion of the low-latitude ionosphere
- High-latitude brightness wave in 630.0 nm airglow observed traveling N-NE to S-SW that encountered the stationary enhancement in the SW
- Empirical Mode Decomposition results on total electron content found wave activity with LSTID characteristics, preceding the optical wave

Correspondence to:
C. Cesaroni,
claudio.cesaroni@ingv.it

Citation:
Cesaroni, C., Alfonsi, L., Pezzopane, M., Martinis, C., Baumgardner, J., Wroten, J., … Umbriaco, G. (2017). The first use of coordinated ionospheric radio and optical observations over Italy: Convergence of high-and low-latitude storm-induced effects. *Journal of Geophysical Research: Space Physics*, *122*. https://doi.org/10.1002/2017JA024325

Received 4 MAY 2017
Accepted 7 SEP 2017
Accepted article online 11 SEP 2017

The First Use of Coordinated Ionospheric Radio and Optical Observations Over Italy: Convergence of High-and Low-Latitude Storm-Induced Effects

C. Cesaroni[1], L. Alfonsi[1], M. Pezzopane[1], C. Martinis[2], J. Baumgardner[2], J. Wroten[2], M. Mendillo[2], E. Musicò[1,3], M. Lazzarin[4], and G. Umbriaco[4]

[1]Istituto Nazionale di Geofisica e Vulcanologia, Rome, Italy, [2]Center for Space Physics, Boston University, Boston, MA, USA, [3]Department of Information, Electronics and Telecommunications, Sapienza University of Rome, Rome, Italy, [4]Department of Physics and Astronomy, University of Padova, Padua, Italy

Abstract Ionospheric storm effects at midlatitudes were analyzed using different ground-based instruments distributed in Italy during the 13–15 November 2012 geomagnetic storm. These included an all-sky imager (ASI) in Asiago (45.8°N, 11.5°E), a network of dual-frequeny Global Navigation Satellite Systems receivers (Rete Integrata Nazionale GPS network), and ionosondes in Rome (41.8°N, 12.5°E) and San Vito (40.6°N, 17.8°E). GPS measurements showed an unusual enhancement of total electron content (TEC) in southern Italy, during the nights of 14 and 15 November. The ASI observed colocated enhancements of 630 nm airglow at the same time, as did variations in N_mF_2 measured by the ionosondes. Moreover, wave-like perturbations were identified propagating from the north. The Ensemble Empirical Mode Decomposition, applied to TEC values revealed the presence of traveling ionospheric disturbances (TIDs) propagating southward between 01:30 UT and 03:00 UT on 15 November. These TIDs were characterized by weak TEC oscillations (~ ±0.5 TEC unit), period of 45 min, and velocity of 500 m/s typical of large-scale TIDs. Optical images showed enhanced airglow entering the field of view of the ASI from the N-NE at 02:00 UT and propagating to the S-SW, reaching the region covered by the GPS stations after 03:00 UT, when TEC fluctuations are very small (~ ±0.2 TEC unit). The enhancement of TEC and airglow observed in southern Italy could be a consequence of a poleward expansion of the northern crest of the equatorial ionization anomaly. The enhanced airglow propagating from the north and the TEC waves resulted from energy injected at auroral latitudes as confirmed by magnetometer observations in Scandinavia.

1. Introduction

In the last several years a growing number of researchers in Europe have investigated ionospheric storm behavior using a multi-instrumental approach to reveal the overall physical environment in which the observed perturbations occur (see, e.g., Alfonsi et al., 2013; Prikryl et al., 2015). In contrast to studies using a single instrument (or clusters of similar instruments), assembling a data set of simultaneous multidiagnostic observations can be a time-consuming process. The science yield, however, can be substantial. Here we report on such an effort that reveals ionospheric disturbance effects from unified radio and optical observations spanning the Italian peninsula. We use radio (L band and HF) and low-light-level optical imaging observations during the geomagnetic storm period of 13–16 November 2012 to show disturbances distinct from the usual positive phase/negative phase patterns associated with N_mF_2 and total electron content variations during ionospheric storms (Mendillo, 2006; Prölss, 1995).

The geomagnetic storm peaking on 14 November 2012 was characterized by a minimum *Dst* index of −118 nT at 08 UT. The storm was caused by a shock due to an interplanetary coronal mass ejection (ICME) that encountered the Earth at about 10 UT on 12 November 2012. Hwang et al. (2015) presented a comprehensive description of solar wind input and magnetospheric effects using in situ data from multiple satellites, ground-based imagers, and magnetometers for the day of the storm's main phase (14 November).

The traditional auroral geomagnetic indices (e.g., *AL* and *AU*) do not show significant activity after ~13 UT on 14 November 2012 (see Figure 1a). At that time, the auroral electrojet index *AE* (defined as *AU-AL*) reached only 800 nT. Most of the solar wind parameters (Figure 1b) did not show significant changes either, with the exception of the solar wind *y* component, B_y, that changed from ~ −4 nT to ~ +4 nT between ~21:40 UT and ~22:00 UT of 14 November, and the solar wind speed V_{SW} that changed from ~410 km/s to

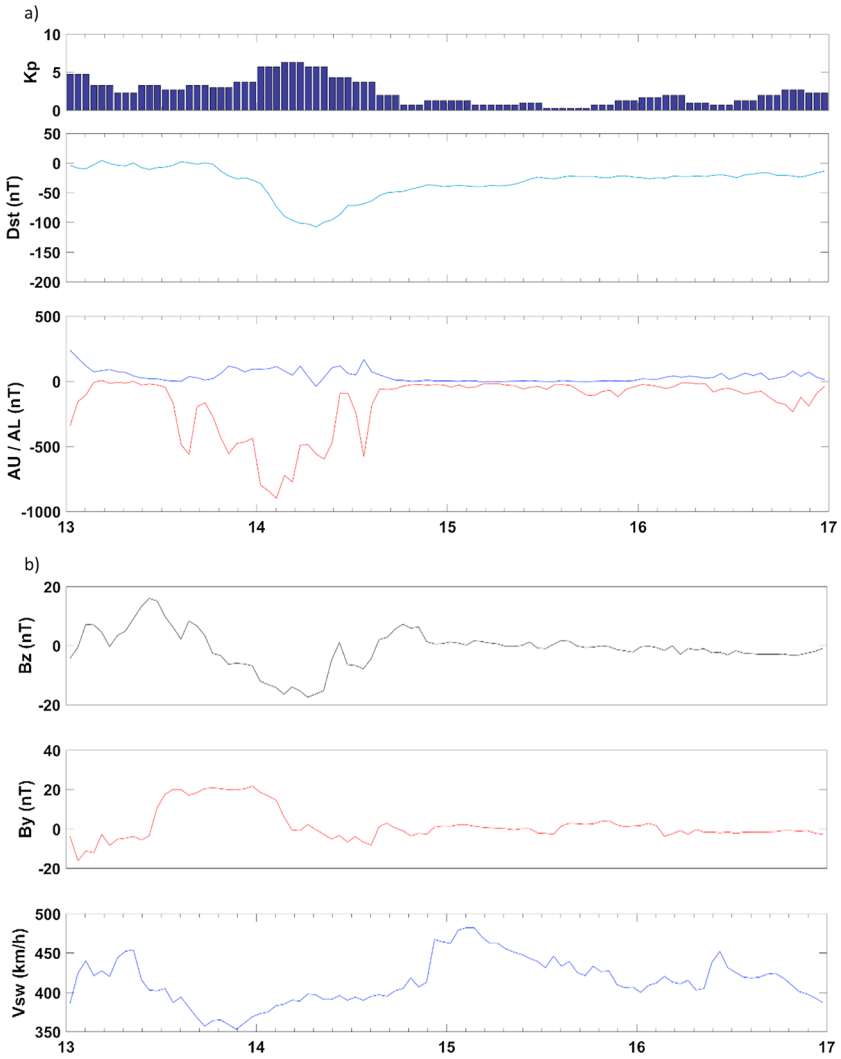

Figure 1. (a) (top) *Kp*, (middle) *Dst*, and (bottom) *AU* and *AL* indices between 13 and 16 November 2012. (b) (top) B_z, (middle) B_y, and (bottom) solar wind speed between 13 and 16 November 2012.

~470 km/s between ~22:00 UT and ~22:20 UT of the same day. We conclude that while the period under study is almost at the end of the recovery phase of the storm, significant activity is observed in the late hours of 14 November.

Here we apply the multidiagnostic approach for ionospheric F_2 layer effects over a 4 day period (13–16) that allows us to detect unusual storm-induced effects on 15 November. We use a network of GPS receivers to provide total electron content (TEC) data and ionosonde stations for the maximum electron density of the F_2 layer (N_mF_2) unified by the broad spatial context provided by an all-sky ionospheric airglow imaging system.

Storm effects include the occurrence of large-scale traveling ionospheric disturbances (LSTIDs) that have been observed at midlatitudes using different instruments (Shiokawa et al., 2002). The cause of LSTIDs has been usually attributed to traveling atmospheric disturbances (TADs) produced by the Joule heating due to the magnetospheric energy deposited in the auroral oval during the storm (Zakharenkova et al., 2016, and references therein). LSTIDs simulations in general predict equatorward wind enhancements, although some studies have shown that poleward wind enhancements at midlatitudes exist after the occurrence of the enhanced equatorward wind (Millward et al., 1993; Shiokawa et al., 2003).

Section 2 describes instrumentation and data analysis methods, section 3 provides results and discussion from each type of observation, and section 4 is devoted to the detection of LSTIDs on 15 November 2012. Conclusions are given in section 5.

2. Instrumentation and Data Analysis Methods

2.1. Total Electron Content From GPS Observations

L band (0.39–1.55 GHz) probing of the ionosphere is a by-product of the information provided by GNSS (Global Navigation Satellite Systems) signals received at ground-level or onboard LEO (low Earth orbit) satellites. Since the ionosphere is a dispersive medium, the use of multifrequency receivers allows TEC to be estimated from the differences between code and/or phase measurements on at least two frequencies. Thus, a dense network of GNSS receivers can provide very high-resolution maps of TEC over a vast region (Cesaroni et al., 2015). The Italian GPS (Global Positioning System) receiver network RING (Rete Integrata Nazionale GPS) is described on the website created by the INGV RING Working Group (2016), http://ring.gm.ingv.it/.

TEC data are reported in column content units (10^{16} el/m^2) called total electron content unit (TECU), with diurnal values at midlatitudes ranging from ~4 to ~30 TECU for solar moderate conditions, with a typical uncertainty on the absolute TEC of few TECU. For this study, a total of about 140 RING stations were used to create maps of TEC, as described in the following section. Calibration of TEC was made by applying the technique introduced by Ciraolo et al. (2007). This method is based on the so-called leveling procedure that allows one to estimate, for each arc of observation associated with a receiver-satellite pair, the biases and all nonzero mean errors (e.g., multipath) that can affect TEC values. The calibrated slant-TEC values are then verticalized (vTEC) by applying the simple $\cos\chi$ mapping function as used by Mannucci et al. (1998), where χ is satellite zenith angle. To produce TEC maps over the Italian region, vTEC values from all stations were interpolated to create grid points (0.1° latitude × 0.1° longitude) by using the natural neighbor technique. As demonstrated by Cesaroni et al. (2015), this method gives a reliable estimate of the TEC distribution when regional datasets are considered.

To address temporal behavior of TEC, the Ensemble Empirical Mode Decomposition (EEMD) method was used to analyze nonlinear and nonstationary time series, based on an adaptive time-frequency decomposition related to a sifting procedure and to the so-called Hilbert-Huang transform (Huang et al., 1998). The EEMD application allows separating a signal into a set of orthogonal and complete functions, the so-called Intrinsic Mode Functions (IMFs). In the present paper, the EEMD is used to discriminate the oscillatory component of vTEC time series from their trends. The former is defined as the sum of the zero-mean IMFs, while the latter is represented by the sum of the remaining IMFs.

2.2. Maximum Electron Densities of the F_2 Layer From Ionosonde Data

High-frequency (HF, 3–30 MHz) radars, known as ionosondes, operate at various sites within Italy, and in nearby European countries. While TEC observations refer to the integral of the ionosphere's electron density profile ($N_e(h)$), ionosondes provide a number of ionospheric parameters obtained using radio reflections from the height of maximum electron density (h_mF_2) and below. The maximum electron density of the ionosphere is derived from the corresponding critical frequency f_oF_2 (according to the relation $N_mF_2 = 1.24 \cdot 10^{10} \cdot (f_oF_2)^2$, where the units of N_mF_2 and f_oF_2 are el$^-$/m^3 and MHz, respectively). In this study we use ionosonde observations from Rome (41.8°N, 12.5°E) and San Vito (40.6°N, 17.8°E) in Italy. The observational accuracy for N_mF_2 is estimated to be $3 \cdot 10^7$ el$^-$/m^3. The behavior of the height of the base of the ionospheric layer, $h'F$, is used to assess vertical motions during the period of study.

The ionosonde at the observing station in Rome is the Advanced Ionospheric Sounder-Istituto Nazionale di Geofisica e Vulcanologia (AIS-INGV) ionosonde (Zuccheretti et al., 2003), and in November 2012 the sounding repetition rate and the sweeping frequency range were respectively set to 15 min and from 1.5 MHz to 15 MHz. The ionospheric station at San Vito is equipped with a Digisonde (Bibl & Reinisch, 1978), and in November 2012 the sounding repetition rate and the sweeping frequency range were set respectively to 15 min and from 1 to 8 MHz, between 17:30 and 03:45 UT (LT = UT + 1), and from 1 to 13 MHz, between 04:00 and 17:15 UT. Data from San Vito were downloaded from the Global Ionospheric Radio Observatory web portal (Reinisch & Galkin, 2011).

For the ionograms recorded at Rome, f_oF_2 values were manually scaled using the Interpre software (Pezzopane, 2004), while for the ionograms from San Vito the f_oF_2 values were manually scaled using the SAO explorer program developed by the University of Massachusetts, Lowell (http://ulcar.uml.edu/SAO-X/SAO-X.html). For each station, the occurrences of spread F phenomena were noted; in most cases, the spread

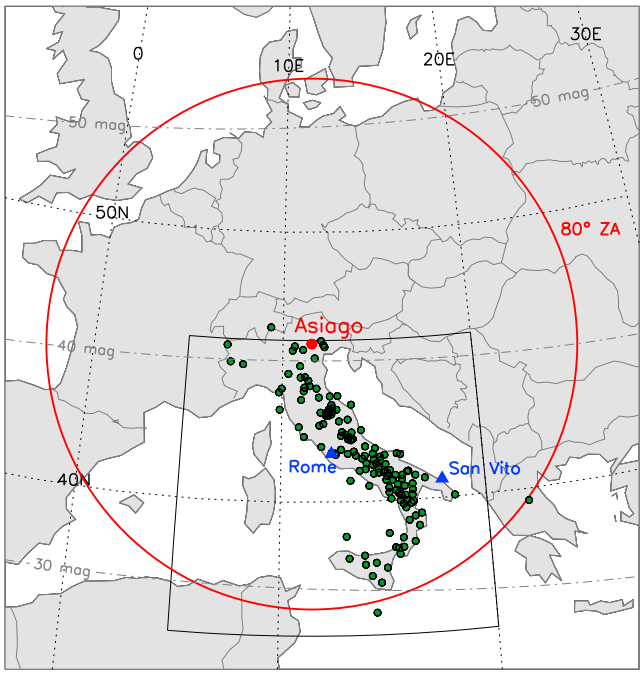

Figure 2. Distribution of the observing instruments used in this study. The field of view of the all-sky imager at the observatory in Asiago is shown for a 630.0 nm airglow emission height of 300 km and zenith angle of 80°. The ~140 stations of the RING network of GPS TEC observations are shown by the green dots. The four-sided region indicated by black lines gives approximately the span of the GPS TEC maps from the RING network. Locations of ionosondes at Rome and San Vito in Italy are indicated by triangles.

F did not prevent the f_oF_2 values from being observed. Finally, for the N_mF_2 values obtained, their corresponding means and standard deviations were calculated for all the days of November 2012 (except the three under investigation).

2.3. F_2 Layer Airglow Patterns From an All-Sky Imager

Low-light level, wide-angle, imaging of subvisual atmospheric emissions are used here to provide the broad spatial context for the line-of-sight ionosonde and GPS observations. An All-Sky-Imaging-Air-Glow-Observatory (ASIAGO) operates at the Cima Ekar station of the Padova Observatory in northern Italy (45.8°N, 11.5°E). This all-sky imager (ASI) is a Boston University-designed instrument described in Baumgardner et al. (2007). The initial results from ASIAGO dealt with subauroral emissions observed during the geomagnetic storm of 26–27 September 2011 (Baumgardner et al., 2013).

The ASIAGO system uses a narrowband filter to capture the oxygen "red line" of 630.0 nm generated by the recombination of ionospheric plasma at a height of approximately 300 km. Areas of brighter versus fainter airglow thus refer to locations in the ionosphere where the electron density is higher versus lower, respectively. This emission is also dependent on the height of the ionospheric layer, so brighter (fainter) airglow occurs when the ionospheric layer moves to lower (higher) altitudes due to increased (reduced) recombination. To create a regional airglow map, the procedure is as follows: each pixel within an image has an elevation angle and azimuth that can be transferred to a geographic map showing latitude and longitude at the height of emission. A 630.0 nm airglow image portrayed from zenith angles of 0° to 80° at 300 km from the ASIAGO site spans vast regions, from northern Africa to southern Scandinavia and from longitudes ~5°W to ~25°E.

Figure 2 summarizes the geographical distribution of the instruments used in this study. All data sets (radio and optical) used are dominated by conditions near the altitude of maximum electron density (h_mF_2 ~ 300 km) making comparisons possible and fruitful.

3. Results

3.1. Ionosonde Observations

The 15 min N_mF_2 values from the Rome and San Vito ionosonde stations are shown in the top and bottom panels of Figure 3, respectively, for the days of 13–15 November 2012 (data for 16 November are not available). The geomagnetic storm onset at ~00 UT on 13 November is followed by a weak positive ionospheric storm in the afternoon hours. Then, through the whole of 14 November 2012, N_mF_2 is depressed well below the lower boundary limit defined by the mean minus the standard deviation. Negative storms like this at midlatitudes are caused by neutral composition changes (Buonsanto, 1999). Specifically, at *F* layer heights this negative phase arises mainly from the decrease in the $[O]/[N_2]$ ratio, which results in a strong ion loss rate enhancement (Prölss, 1995).

This composition disturbance zone propagates equatorward from the auroral region with the disturbance meridional neutral wind of the storm (Skoblin & Förster, 1995; Zuzic et al., 1997). Daytime N_mF_2 values recover to their typical values on 15 November 2012. For a winter season ionospheric storm, a strong daytime negative phase is somewhat unusual when TEC data are used from stations near ~70 W (Mendillo, 2006). Yet a quick recovery of the negative phase for a winter storm, as shown here, is fully consistent with past results (Mendillo, 2006; Prölss, 1995).

Ionospheric storm disturbances observed during nighttime hours can be quite different from daytime effects (Mendillo, 2006). The most often recorded F_2 layer effects at midlatitudes are nighttime increases in peak electron density. This occurred between 00 and 04 UT on both 14 and 15 November. In this paper we

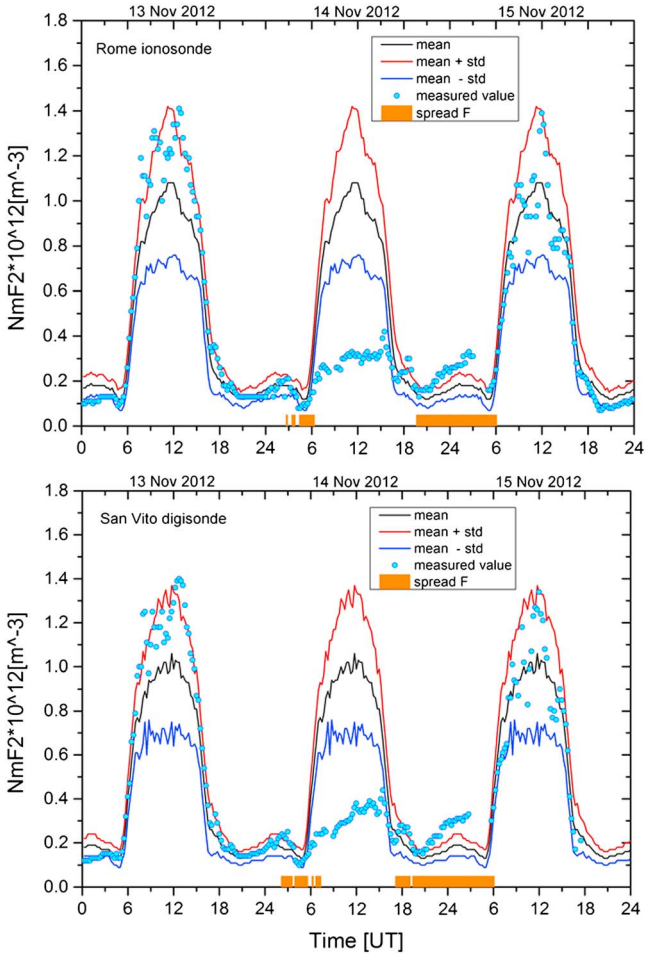

Figure 3. N_mF_2 as measured (light blue dots) at (top) Rome and (bottom) San Vito from 13 to 15 November 2012, together with the corresponding mean (black curve) and standard deviation (red and blue curves above and below the mean curve represent the mean ± the standard deviation, respectively) calculated considering all the days of November 2012 (except 13–15). Orange vertical bars at the bottom of each panel highlight the presence of spread *F* phenomena on the ionogram.

concentrate on the N_mF_2 values between 00 and 03 UT on 15 November 2012, when they are anomalously well above their upper limits defined by the mean plus the standard deviation. At the same time, all the corresponding ionograms are characterized by midlatitude spread *F*.

3.2. Optical Observations

Figure 4 shows four all-sky images taken at ~02 UT from 13 to 16 November 2012. Figures 4c and 4d (15 and 16 November) have clear skies, while Figure 4a (13 November) is partially clear and Figure 4b (14 November) is mostly cloudy. On November 13 (Figure 4a) the 630.0 airglow is very uniform with no particularly interesting features (e.g., latitude gradients) at ~02 UT. The image on November 15 (Figure 4c), however, shows two areas with bright 630.0 nm emission: one to the north and northeast (N-NE), and the other one to the south-southwest (S-SW). The latter bright feature coincides with the anomalous nighttime N_mF_2 increases found at both ionosonde sites in Figure 3. Figure 4d shows bright airglow only to the N-NE.

3.3. TEC Observations

Figure 5 shows RING TEC maps for the same time (~2:05 UT) on each night to compare with the images in Figure 4. There are regions of enhanced nighttime TEC at levels of 12–14 TECU recorded on 15 November that coincide with the spatial pattern of airglow enhancements visible to the S-SW in Figure 4c. Moreover, the TEC maps clearly show the lack of enhancements during the nights of 13 and 16 November. Enhanced TEC values were observed on 14 November. The ionosonde data in Figure 3 show these enhancements in N_mF_2 during the same 02–03 UT hours on 14 and 15, the latter being significantly larger. The optical data from ASIAGO show only the concurrent pattern for 15 due to cloudy skies on 14.

With the GPS TEC data available at a much higher time resolution than the optical data, we were able to conduct a detailed investigation of vTEC oscillating components. This was done by means of the EEMD method and the continuous wavelet transform using a Morlet mother wavelet. Figure 6 (top) shows the spectrum of the vTEC oscillating component from 13 to 16 November 2012 obtained from the GPS receiver installed in Rome (41.83°N, 12.51°E). The analysis offers evidence of a periodicity of ~1 h on 14 and 15 November 2012, around 04 UT and 00 UT, respectively. A larger signal is observed on 15 November 2012, around 02 UT, with a periodicity of ~45 min.

4. Discussion

In order to interpret our observations, i.e., increased airglow patterns, increased TEC from regional maps, and the presence of TEC perturbations, we will focus on these particular signatures measured on 15 November.

4.1. Enhanced TEC

The enhancements in TEC on 14 and 15 November could be related to unusual poleward excursions of low latitude ionospheric morphology. Such high TEC values for nighttime conditions are certainly unusual for midlatitudes, but not so at typical location of the equatorial ionization anomaly (EIA). The fact that the nighttime increases in N_mF_2 were not obscured by the moderate spread *F* in ionosonde data suggests that extra ionization created by energetic particle precipitation can be ruled out since they would have created scintillations and strong spread *F* for such high nighttime TEC values (12–14 TECU). Joseph et al. (2015) described TEC values from East Africa during this November 2012 storm using GPS stations located mostly south of the geomagnetic equator. During the 00–02 UT period on 14 and 15 November, TEC values were ~20 TECU at

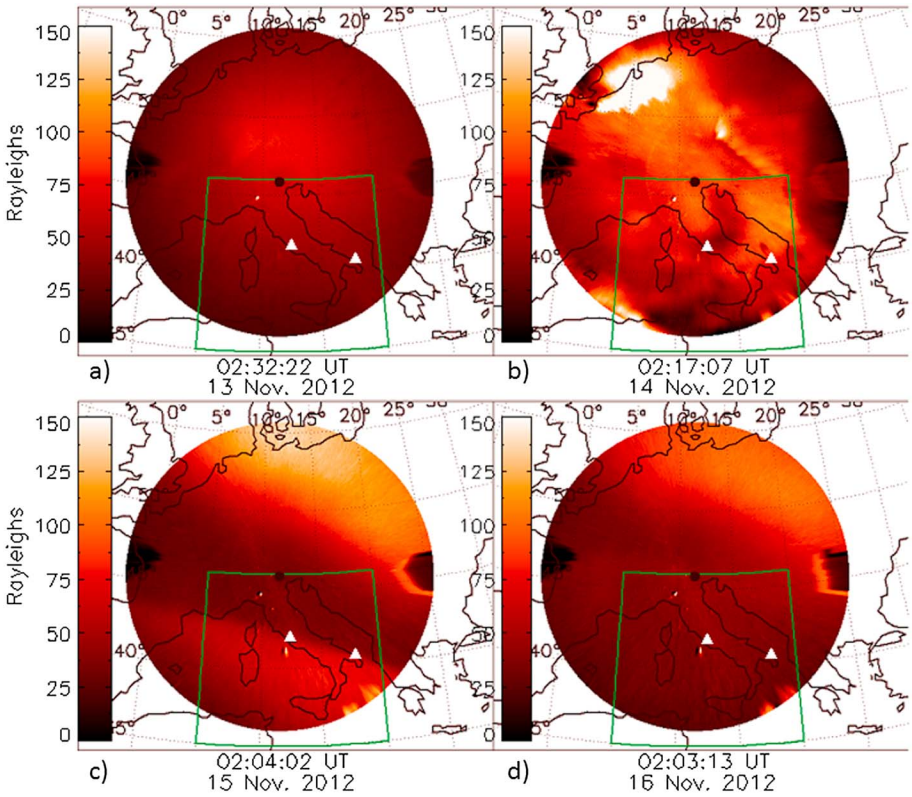

Figure 4. All-sky images of 630.0 nm emission from the ASIAGO observatory, taken at ~02 UT from 13 to 16 November 2012, which are to be compared with the TEC maps shown in Figure 5.

locations ~25°S in latitude south of the geomagnetic equator. Since in this longitude sector the difference between geomagnetic and geographical latitude is about 10°, such a pattern is consistent with our findings at approximately the same conjugate magnetic latitudes in the northern hemisphere. Nevertheless, the mechanism that would cause such excursions of equatorial morphologies into lower midlatitudes well into the storm recovery phase periods remains elusive. Rishbeth et al. (2010) hypothesized that transport from lower latitudes might not be the source of additional ionization at midlatitudes. They proposed that local changes in ionization production could be an important process for producing plasma density enhancements at midlatitudes; this would then affect observations in the nighttime hours. Their argument was based on the fact that even during superstorms the plasma at low latitudes would not be able to "travel" far enough in their lifetime to produce density enhancements at midlatitudes. This interpretation was objected by Tsurutani et al. (2013) who tried to validate the hypothesis of midlatitude plasma enhancements caused by the transport of low-latitude plasma.

During 13–16 November the Defense Meteorological Satellite Program (DMSP) F17 satellite passed near the longitude sectors sampled by the ASI around 04:30 UT. Figure 7a shows the southward trajectories of satellite F17 during the four nights at a height close to 850 km with respect to the ASI field of view. Figure 7b shows in situ ion density (Ni) values from +50° magnetic latitude to −50° magnetic latitude. The nights of 14, 15, and slightly of 16 November show Ni increases near ~20°–25° magnetic latitude on Northern Hemisphere and ~30°–35° magnetic latitude on Southern Hemisphere. This suggests that low-latitude electrodynamics could have played a significant role in increasing N_mF_2 and TEC as depicted by Figures 3 and 5. Figure 7c focuses on Ni data after mapping the satellite trajectory along *B* field lines to a height of 300 km between 30° and 55°N. The 13 November data, shown in dotted lines, indicate relatively uniform ion densities in the latitude range covered by the ASI. The 15 November data, shown in solid thick lines, present a region of elevated ion densities between ~32° and ~37°N and a region of decreased ion densities, between ~37° and ~44°N. These observations help to interpret the optical signatures from the ASI and the GPS TEC regional maps, to be discussed in section 4.3 below.

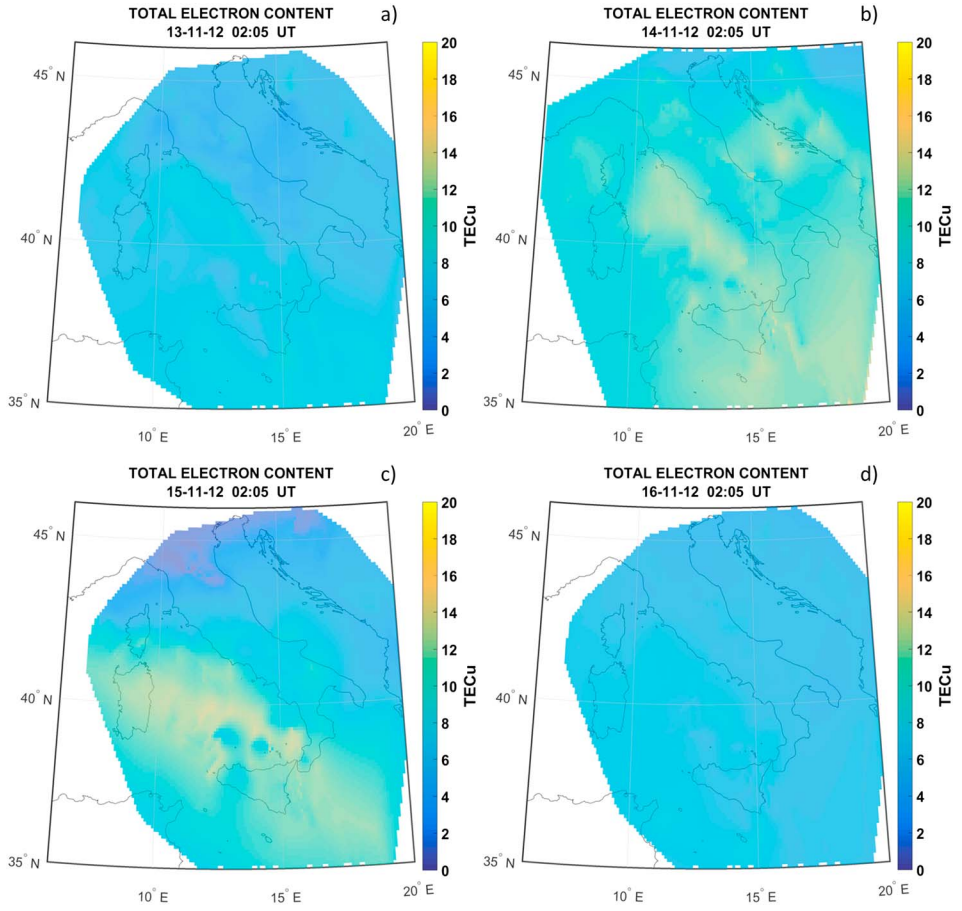

Figure 5. Maps of calibrated vTEC, computed at 02:05 UT from 13 to 16 November 2012 using data acquired from all the available RING GNSS stations. These times match those of the optical images in Figure 4.

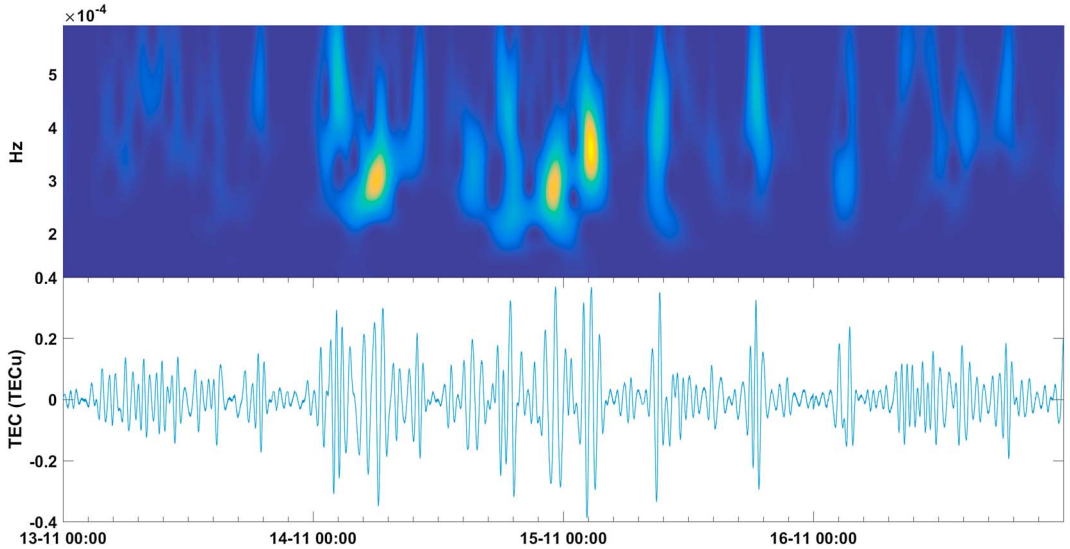

Figure 6. (top) Wavelet spectrum of the (bottom) TEC oscillating component obtained after applying the EEMD method on vTEC signal from the GPS station (ingr) installed at Rome from 13 to 16 November 2012. Blue line in Figure 6 (bottom) represents the same signal as the blue line in Figure 9.

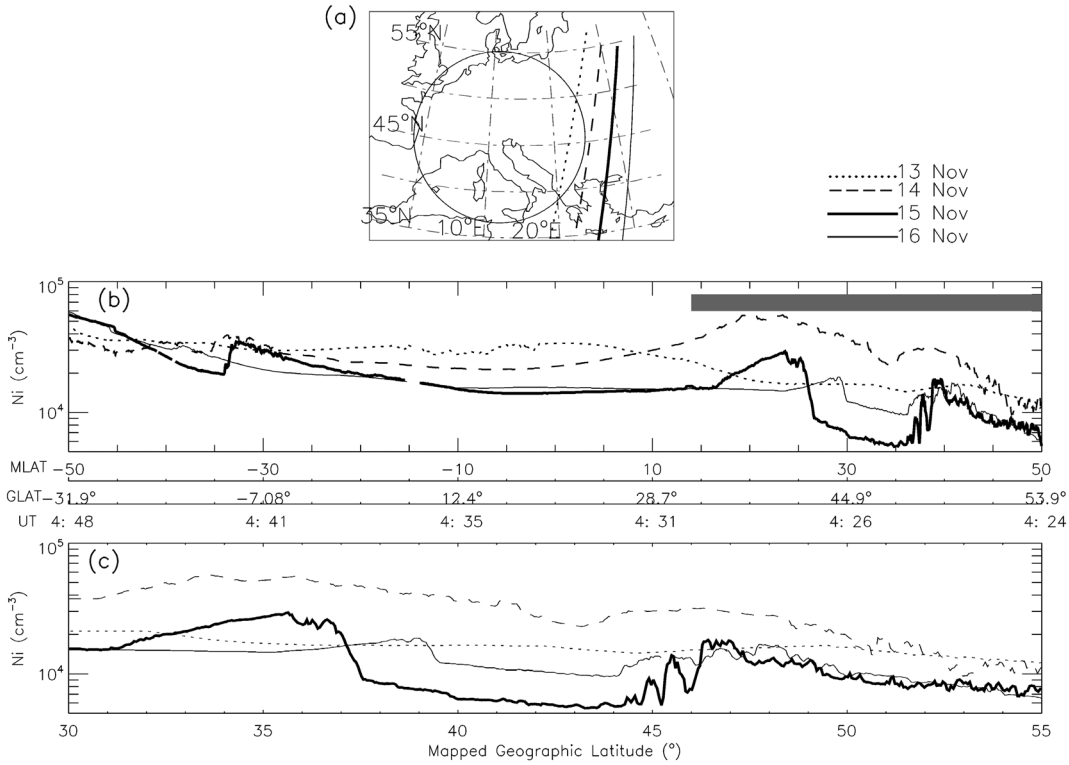

Figure 7. (a): DMSP F17 passes on 13 November (dotted), 14 November (dashed), 15 November (thick solid), and 16 November (solid). The circle represents the FOV of the ASI; (b) in situ ion density values showing large values in the Northern Hemisphere during 14 and 15 November the gray rectangle between ~15 and 50 magnetic latitude represents the region zoomed in the bottom panel; (c) ion density values mapped to a height of 300 km in the latitude region covered by the ASI's field of view. Increased values are observed on 15 November between ~32° and ~37°; a net reduction is observed between ~37° and ~44° (see text).

4.2. Optical and GPS Detection of Large-Scale Waves

Figure 8 gives a set of 630.0 nm images for the period 02:04–04:35 UT on 15 November 2012. The unusual high brightness to the S-SW remained quasi-stable, with a very small southward motion. This quasi-stationary enhancement is seen from ~22:00UT on 14 November 2012. Another feature seen is a region of increased airglow propagating from the N-NE to the S-SW, named a "high-latitude brightness wave (HLBW)". This HLBW appeared in Figure 4c at latitudes outside of the RING network coverage and therefore not captured in the TEC data shown in Figure 5c. The sequence of images in Figure 8 shows that the HLBW propagates to the south, reducing the dark airglow region that separates the quasi-stationary bright airglow feature in the southwest. The orientation of the HLBW is initially tilted with respect to the fixed airglow enhancement, but by 4:16 UT both structures are similarly aligned. We also notice a thin area of dark airglow spanning from ~50° to ~47°N at 3:13 UT.

We next apply the EEMD method to the vTEC values computed on 15 November between 01:30 and 6:00 UT at three RING stations: Teolo (45.20°N, 11.40°E), Rome (41.83°N, 12.51°E), and Corleone (37.89°N, 13.30°E). This method is a useful tool to learn how any potential waves might be moving over Italy in terms of direction and velocity. Figure 9 shows vTEC oscillating components related to the three stations. A clear southward motion in the vTEC perturbations is observed between 01:30 and 02:15 UT. After this time the coherence between vTEC perturbations observed first in the northernmost station and later in the southern sites is weaker, although some wave activity could be inferred between ~02:30 and 03:00 UT. We can estimate that during the 01:30 to 02:15 UT interval the perturbation in vTEC moves with a speed of the order of 500 m/s. This wave can be related to the peak period of ~45 min shown in Figure 6. An estimate of the horizontal wavelength from the obtained velocity (500 m/s) and period (45 min) gives a value of about 1350 km, which is consistent with the propagation of LSTIDs (Hunsucker, 1982). The waves determined by the EEMD method seem to dissipate after ~3:30 UT.

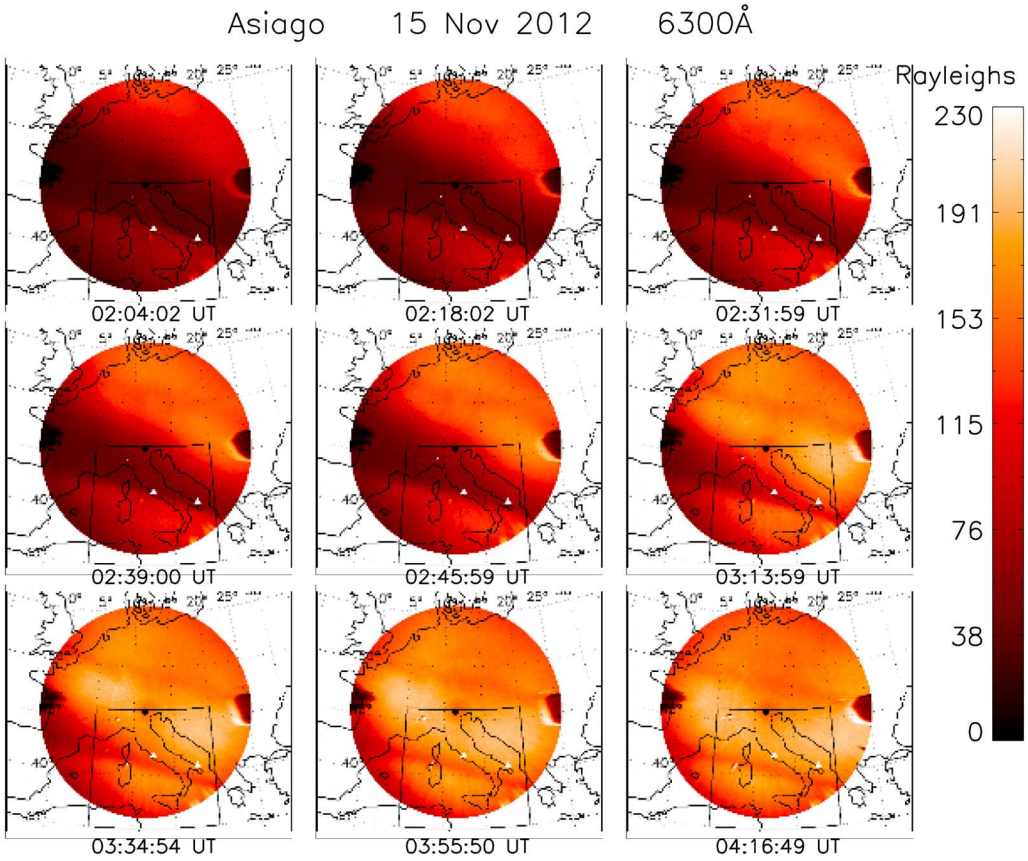

Figure 8. A series of nine all-sky images in 630.0 nm emission spanning the time from 02:04 UT to 04:16 UT on 15 November 2015. Note that the enhanced emission that starts in the N-NE moves toward the S-SW but never exceeds the latitude of the quasi-stationary airglow enhancement to the south. The orientation of the high-latitude brightness wave is initially tilted with respect to the airglow enhancement to the south. White triangles indicate the ionosonde stations at Rome and San Vito.

4.3. An Overall Interpretation

Ionosonde data from 13 November to 16 November confirm our general understanding of ionospheric storm effects at midlatitudes. The results are summarized in Figure 3, where the typical positive and negative phases are observed. Focusing on the night of 15 November 2012, very late into the recovery phase, when storm activity was practically null, ionosonde data measured elevated N_mF_2 between 00 and 03 UT. After this time spread *F* affected the ionosonde measurements and no N_mF_2 observations were possible. The optical data show an almost quasi-stationary enhanced airglow to the south during the entire night of 15 November and a southward propagating structure after ~2:00 UT that reached the Rome and San Vito ionosonde stations around 03:00–3:30 UT. Regional TEC maps from the RING network revealed enhanced values at ~02:00 UT coincident with the optical data that showed increased brightness to the south. In addition, the EEMD technique applied to a set of GPS receivers shows the presence of waves that seem to occur before the southward propagating feature.

DMSP data provide supporting information that if mapped to the height of the airglow layer can help in the interpretation of the phenomena observed. The quasi-stationary bright airglow occurs in a region that also shows enhanced TEC (Figure 5), abnormally high N_mF_2 (Figure 3), and elevated in situ ion density (Figure 7). It is not clear what the source of these elevated values at midlatitudes is. It might be, as we discuss later, that isolated substorm effects could be providing electric field perturbations that modify the plasma environment at global scales in ways not completely understood (Rishbeth et al., 2010).

For the S-SW propagating structure the variations in brightness of the 630.0 nm emission in Figure 8 is about 100 rayleighs (R) above background, easily seen in the images. The changes in TEC at the time of such strong

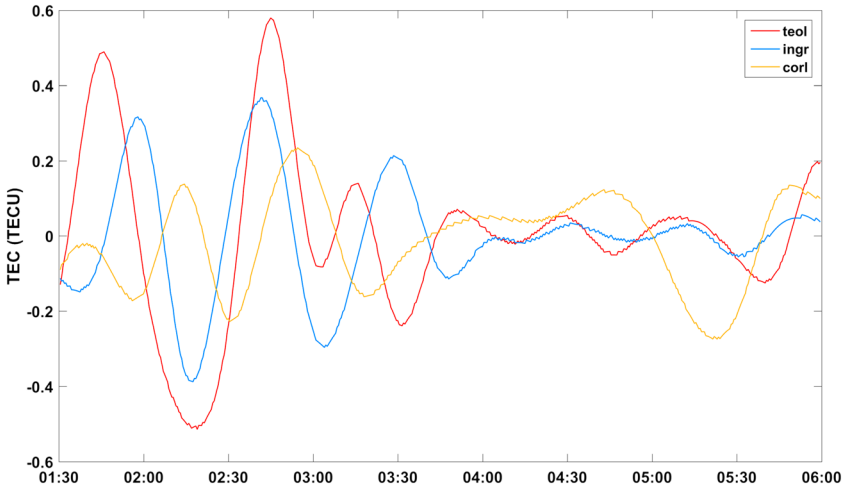

Figure 9. TEC oscillating components from teol (45.20°N, 11.40°E, red line), ingr (41.83°N, 12.51°E, blue line), and corl (37.89°N, 13.30°E, yellow line) stations on 15 November between 01:30 and 6:00 UT. Oblique lines connect the peaks of the vTEC oscillatory components that are used to evaluate the velocity of the wavy perturbation along the path teol-ingr (black thick line) and ingr-corl (green thick line).

increase in airglow are less than ~0.2 TECU (see Figure 9). Moreover, the full representation of TEC as function of UT time and geographic latitude does not show any enhancement propagating southward after ~3:00 UT (Figure 10). If no enhancement causes the increased 630.0 nm airglow we are left then with a lowering of the electron density profile into the dense neutral atmosphere as the cause of the 630.0 nm enhancement. Ionosonde data can help to investigate if a layer descent occurred during this event. The pattern of brightness propagating from the N-NE reaches San Vito between 2:30 and 3:30 UT. During this period strong spread *F* was present, but we could still manually validate the height of the ionospheric *F* layer (*h*′*F*) for both Rome and San Vito ionograms. Values of *h*′*F* recorded on 14 and 15 November 2012 are superposed on TEC values in Figure 10. Specifically, the San Vito data (black dashed curve) shows that *h*′*F* changed from ~250 km at 2:15 UT to ~210 km at 3:00 UT, a variation in height sufficient to produce the dramatic increase in brightness. A similar behavior was also observed by the Rome *h*′*F* data (red curve). The DMSP data at ~4:30 UT (see Figure 7) shows depleted ion density in the latitude range corresponding to the enhanced brightness that propagated from the N-NE. This implies that plasma from ~850 km (the height of the DMSP satellite orbit) moves to lower altitudes, causing a descent in the height of the ionospheric layer and a subsequent enhanced airglow.

We now turn to the high-latitude brightness wave propagating to the southwest. Shiokawa et al. (2002) were able to measure downward plasma motion when trying to explain a purely southward motion of enhanced airglow that coincided with a perturbation in TEC values of the order of 0.2–0.5 TECU (2–6% of the background values) that had all the characteristics of large-scale traveling ionospheric disturbances. The equatorward propagation of the airglow brightness and the descent of the height of the ionospheric layer were explained by a net reduction, or a reversal, of a southward wind present during the night. This seems in principle to be contrary to the view of enhanced equatorward winds originated from the auroral regions. But some LSTID simulations predict poleward wind enhancements after the passage of an initial equatorward wind (Millward et al., 1993).

In the case we are studying, LSTIDs determined by the EEMD method are observed before the high-latitude brightness wave. While the amplitudes of the TEC variations are similar to the ones observed as LSTID in the Japanese sector during the magnetic storm of 15 September 1999, these variations do not seem to be related to the propagating airglow feature. This is in contrast with the results of Shiokawa et al. (2002, 2003), who showed the passage of a single pulse in TEC variations coincident with the passage of an equatorward moving brightness wave. For our 15 November case, where background values are ~20 TECU, the TEC variations measured after 03 UT are less than ~0.2 TECU, just ~1% of the background TEC values, much smaller than the ones observed by Shiokawa et al. (2002). The very small TEC perturbations after ~3:00 UT, measured by the GPS stations from the RING network, could be related to the HLBW.

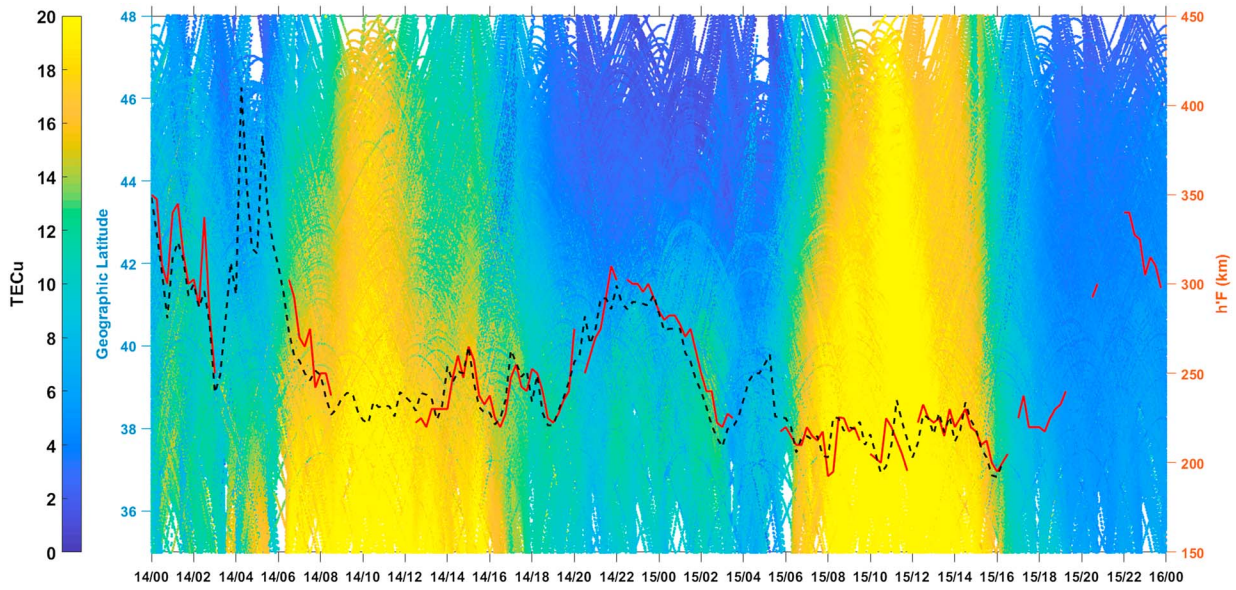

Figure 10. TEC representation as function of UT time and geographic latitude during 14–15 November 2012. Red and black dashed curves represent *h'F* values recorded at Rome and San Vito, respectively.

As seen in Figure 1 between ~00 and 04 UT, magnetic indices do not show any activity. Using the International Monitor for Auroral Geomagnetic Effects (IMAGE) magnetograms we show the *X* component of the Earth's magnetic field from 18:00 UT on 14 to 02:00 UT on 15 UT from high-latitude stations between ~10° and 20°E. Figure 11 shows a map with the locations of the sites (left) and the corresponding *B* field *X* component (right). Most of the activity occurs between ~00:00 UT and 00:30 UT, between ~72° and 68°N, with practically no perturbations below 68°N. The waves measured in Italy were probably

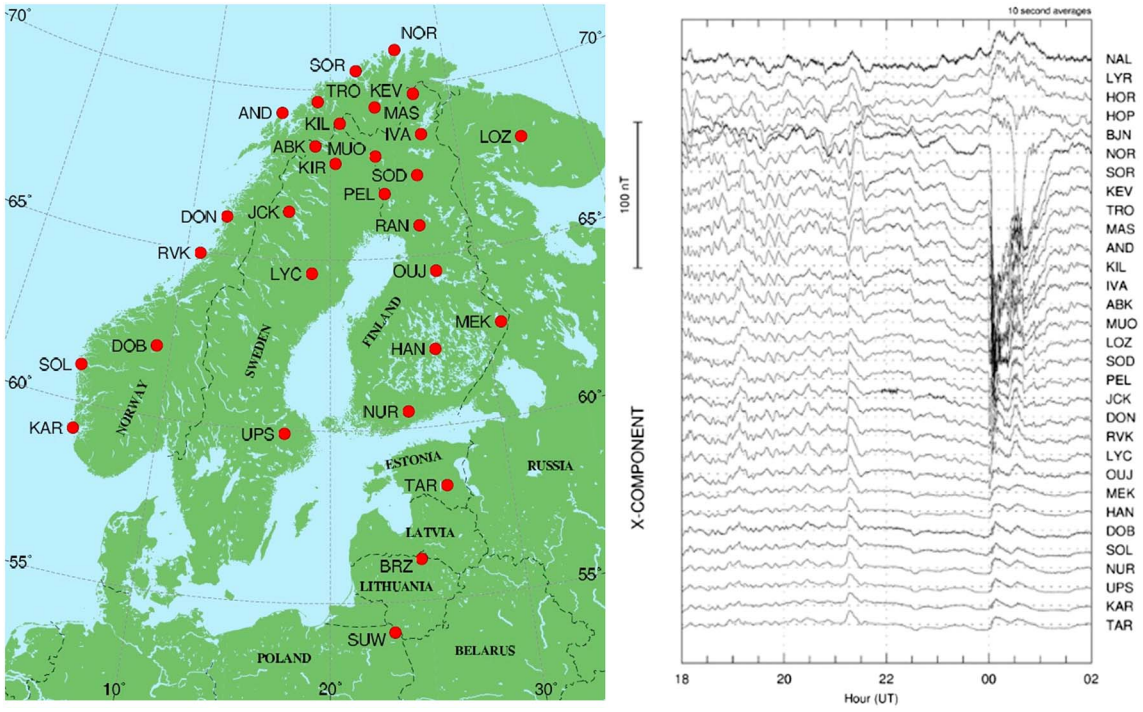

Figure 11. (left) Magnetometer stations from IMAGE covering ~10°–30°E; (right) *x* component of the *B* field showing strong perturbations near 00 UT only between ~68° and ~72°. The five northernmost stations are not reported on the map in Figure 11 (left).

generated by energy input at these auroral stations. If we consider the time it takes a perturbation generated at ~68°N at ~00:15 UT to reach ~45°N, the northern GPS station used in the EEMD method that showed a TEC perturbation of ~0.5 TECU at ~01:45 UT, we obtain a speed of ~470 m/s, similar to the value obtained from Figure 9. Thus, we can identify the localized energy source generating the waves determined by the EEMD method. The amplitude of the TEC waves is too small to produce a significant effect in the airglow brightness; thus, no airglow perturbations are seen between ~01:00 and 02:00 UT in the field of view covering the location of the GPS stations. The HLBW moves through the field of view at a speed of ~300 m/s, smaller than the speed of the perturbations determined by the EEMD method. We believe that this wave could also be considered a LSTID that moves slower and is affected by the presence of the enhanced region to the south of the ASI.

5. Conclusions

A multidiagnostic approach using the first coordinated analyses of ionospheric radio and optical measurements taken over Italy has revealed ionospheric features observed at the end of the recovery phase of a moderate geomagnetic storm in November 2012. The main outcomes of this work are focused on early 15 November (00–04 UT) and are summarized below:

1. An unusual increase of ionospheric plasma density was clearly observed over southern Italy by both optical and radio systems. The F_2 layer enhancements in peak density, total electron content, and airglow brightness persisted almost stationary for several hours. From Figures 3–5 these enhancements are, respectively, $\Delta N_{max} \sim 2 \times 10^{11}$ e^-/m^3 (~100%), Δ6300 Å ~ 50 R (~100%), and ΔTEC ~ 12–14 TECU (≥ 100%). Such enhancements are also confirmed by satellite data from DMSP F17 at ~04:25 UT showing ion density variations on 15 November that included elevated in situ Ni (Figure 7), consistent with the interpretation of enhanced N_mF_2, GPS-derived TEC, and 630.0 nm airglow near 35°N. While no conclusive evidence points to the source of this enhancement, we associate this effect with the intrusion of low-latitude ionospheric morphology into the Mediterranean region.
2. The time history of optical measurements from ~02:00 UT to ~04:00 UT revealed a "high-latitude brightness wave" in 630.0 nm airglow traveling from the N-NE to the S-SW that did not penetrate the stationary enhancement observed to the south. This HLBW with Δ6300 Å ~ 100 R ~ 100% was triggered by an auroral energy injection as confirmed by the high-latitude magnetograms in the Scandinavian sector between 72°N and 68°N. With no significant TEC variations observed, the HLBW is associated with plasma moving to lower heights and producing the increased 630.0 nm airglow pattern. This is consistent with DMSP depleted Ni values observed between ~38° N and 44°N. The HLBW resembles the LSTID observed by Shiokawa et al. (2002, 2003) although it is not accompanied by large TEC variations, it does not propagate just southward, and it is observed at the end of the recovery phase of the storm.
3. Auroral activity was also responsible for the presence of small-amplitude TEC waves propagating at about 500 m/s and wavelength of ~1350 km typical of LSTIDs, revealed by the application of the EEMD method to TEC measurements from ground-based GPS stations

Acknowledgments
We are grateful to the GIRO working group for making the San Vito ionosonde data available at http://spase.info/SMWG/Observatory/GIRO and to the INGV RING working group for making available the GPS data. We thank Kyoto University for providing magnetic indices data and the FMI for maintaining the IMAGE Magnetometer Array. At Boston University, this work was funded, in part, by grants from the National Science Foundation (AGS-1123222, M. M.; AGS-1552301, C. M.; OPP-1246423, C. M.; AGS-1552045, J. B.). M. M. acknowledges sabbatical support from BU. Quick-look images and movies of ASIAGO can be found at www.buimaging.com. At Istituto Nazionale di Geofisica e Vulcanologia this work is partially funded by IONORING project.

References

Alfonsi, L., Spogli, L., Pezzopane, M., Romano, V., Zuccheretti, E., De Franceschi, G., … Ezquer, R. G. (2013). Comparative analysis of spread-*F* signature and GPS scintillation occurrences at Tucumán, Argentina. *Journal of Geophysical Research: Space Physics*, *118*, 4483–4502. https://doi.org/10.1002/jgra.50378

Baumgardner, J., Wroten, J., Mendillo, M., Martinis, C., Barbieri, C., Umbriaco, G., … Hairston, M. (2013). Imaging space weather over Europe. *Space Weather*, *11*, 69–78. https://doi.org/10.1002/swe.20027

Baumgardner, J., Wroten, J., Semeter, J., Kozyra, J., Buonsanto, M., Erickson, P., & Mendillo, M. (2007). A very bright SAR arc: Implications for extreme magnetosphere-ionospher coupling. *Annales de Geophysique*, *25*, 2593–2608.

Bibl, K., & Reinisch, B. W. (1978). The universal digital ionosonde. *Radio Science*, *13*, 519–530. https://doi.org/10.1029/RS013i003p00519

Buonsanto, M. J. (1999). Ionospheric storms—A review. *Space Science Reviews*, *88*, 563–601.

Cesaroni, C., Spogli, L., Alfonsi, L., De Franceschi, G., Ciraolo, L., Monico, J. F. G., … Bougard, B. (2015). L-band scintillations and calibrated total electron content gradients over Brazil during the last solar maximum. *Journal of Space Weather and Space Climate*, *5*, A36.

Ciraolo, L., Azpilicueta, F., Brunini, C., Meza, A., & Radicella, S. M. (2007). Calibration errors on experimental slant total electron content (TEC) determined with GPS. *Journal of Geodesy*, *81*, 111–120. https://doi.org/10.1007/s00190-006-0093-1

Huang, N. E., Shen, Z., Long, S. R., Wu, M. C., Shih, H. H., Zheng, Q., … Liu, H. H. (1998). The empirical mode decomposition and the Hilbert spectrum for nonlinear and non-stationary time series analysis. *Proceedings of the Royal Society of London A: mathematical, physical and engineering sciences*, *454*, 903. https://doi.org/10.1098/rspa.1998.0193

Hunsucker, R. D. (1982). Atmospheric gravity waves generated in the high-latitude ionosphere: A review. *Reviews of Geophysics*, *20*, 293–315. https://doi.org/10.1029/RG020i002p00293

Hwang, K.-J., Sibeck, D. G., Fok, M.-C. H., Zheng, Y., Nishimura, Y., Lee, J.-J., … Onsager, T. (2015). The global context of the 14 November 2012 storm event. *Journal of Geophysical Research: Space Physics*, *120*, 1939–1956. https://doi.org/10.1002/2014JA020826

INGV RING Working Group (2016). Rete integrata Nazionale GPS, https://doi.org/10.13127/RING

Joseph, O. O., Yamazak, Y., Cilliers, P., Baki, P., Ngwira, C. M., & Mito, C. (2015). A study on the response of the Equatorial Ionization Anomaly over the East Africa sector during the geomagnetic storm of November 13, 2012. *Advances in Space Research*, *55*(12), 2863–2872.

Mannucci, A. J., Wilson, B. D., Yuan, D. N., Ho, C. H., Lindqwister, U. J., & Runge, T. F. (1998). A global mapping technique for GPS-derived ionospheric total electron content measurements. *Radio Science*, *33*, 565–582. https://doi.org/10.1029/97RS02707

Mendillo, M. (2006). Storms in the ionosphere: Patterns and processes for total electron content. *Reviews of Geophysics*, *44*(4), RG4001. https://doi.org/10.1029/2005RG000193

Millward, G. H., Moffett, R. J., Quegan, S., & Fuller-Rowell, T. J. (1993). Effects of an atmospheric gravity wave on the midlatitude ionospheric *F* layer. *Journal of Geophysical Research*, *98*(A11), 19173–19179. https://doi.org/10.1029/93JA02093

Pezzopane, M. (2004). Interpre: A Windows software for semiautomatic scaling of ionospheric parameters from ionograms. *Computational Geosciences*, *30*, 125–130. https://doi.org/10.1016/j.cageo.2003.09.009

Prikryl, P., Ghoddousi-Fard, R., Spogli, L., Mitchell, C. N., Li, G., Ning, B., … Jayachandran, P. T. (2015). GPS phase scintillation at high latitudes during geomagnetic storms of 7–17 March 2012—Part 2: Interhemispheric comparison. *Annales Geophysicae*, *33*, 657–670, 2015.

Prölss, G. W. (1995). Ionospheric *F*-region storms. In H. Volland (Ed.), *Handbook of atmospheric electrodynamics* (Vol. 2, pp. 195–248). Boca Raton: CRC Press.

Reinisch, B. W., & Galkin, I. A. (2011). Global ionospheric radio observatory (GIRO). *Earth, Planets and Space*, *63*, 377–381. https://doi.org/10.5047/eps.2011.03.001

Rishbeth, H., Heelis, R. A., Makela, J. J., & Basu, S. (2010). Storming the Bastille: The effect of electric fields on the ionospheric *F*-layer. *Annales de Geophysique*, *28*, 977–981. https://doi.org/10.5194/angeo-28-977-2010

Shiokawa, K., Otsuka, Y., Ogawa, T., Balan, N., Igarashi, K., Ridley, A. J., … Yumoto, K. (2002). A large-scale traveling ionospheric disturbance during the magnetic storm of 15 September 1999. *Journal of Geophysical Research*, *107*(A6), SIA 5-1–SIA 5-11. https://doi.org/10.1029/2001JA000245

Shiokawa, K., Otsuka, Y., Ogawa, T., Kawamura, S., Yamamoto, M., Fukao, S., … Yumoto, K. (2003). Thermospheric wind during a storm-time large-scale traveling ionospheric disturbance. *Journal of Geophysical Research*, *108*(A12), 1423. https://doi.org/10.1029/2003JA010001

Skoblin, M. G., & Förster, M. (1995). Steep latitudinal gradients of thermospheric composition during magnetic storms: A possible formation mechanism. *Annales de Geophysique*, *13*, 277–284.

Tsurutani, B. T., Mannuccci, A. J., Verkhoglyadova, O. P., & Lakhina, G. S. (2013). Comment on "Storming the Bastille: The effect of electric fields on the ionospheric *F*-layer" by Rishbeth et al. (2010). *Annales de Geophysique*, *31*, 145–150. https://doi.org/10.5194/angeo-31-145-2013

Zakharenkova, I., Astafyeva, E., & Cherniak, I. (2016). GPS and GLONASS observations of large-scale traveling ionospheric disturbances during the 2015 St. Patrick's Day storm. *Journal of Geophysical Research: Space Physics*, *121*, 12,138–12,156. https://doi.org/10.1002/2016JA023332

Zuccheretti, E., Tutone, G., Sciacca, U., Bianchi, C., & Arokiasamy, B. J. (2003). The new AIS-INGV digital ionosonde. *Annales Geophysicae Italy*, *46*(4), 647–659.

Zuzic, M., Scherliess, L., & Prölss, G. W. (1997). Latitudinal structure of thermospheric composition perturbations. *Journal of Atmospheric and Solar-Terrestrial Physics*, *59*, 711–724.